
Article:
Charreau, J., Saint-Carlier, D., Lavé, J. et al. (7 more authors) (2018) Late Pleistocene acceleration of deformation across the northern Tianshan piedmont (China) evidenced from the morpho-tectonic evolution of the Dushanzi anticline. Tectonophysics, 730. pp. 132-140. ISSN 0040-1951

https://doi.org/10.1016/j.tecto.2018.02.016

Late Pleistocene acceleration of deformation across the northern Tianshan piedmont (China) evidenced from the morpho-tectonic evolution of the Dushanzi anticline

Julien Charreau[1], Dimitri Saint-Carlier[1], Jérôme Lavé[1], Stéphane Dominguez[2], Pierre-Henri Blard[1], Jean-Philippe Avouac[3], Nathan David Brown[4], Luca Claude Malatesta[3], Wang Shengli[5] and Edward Rhodes [3]

1. Centre de Recherche Pétrographique et Géochimique.-, Université de Lorraine - CNRS, , UMR 7358, 15 rue Notre Dame des Pauvres, B.P. 20, 54501 Vandœuvre lès Nancy, France
2. University of Montpellier, Géosciences Montpellier, UMR 5243, Place E. Bataillon, case 060 - 34095 Montpellier Cedex 5, France
3. California Institute of Technology, Division of Geology and Planetary Sciences, 1200 E California Blvd, Pasadena CA 91125, United States
4. University of California, Department of Earth, Planetary and Space Sciences, Los Angeles, California 90095-1567, United States
5. Nanjing University, Department of Earth and Sciences, Nanjing, China

Keys words: tectonic; shortening rates; Dushanzi Kuitun; Tianshan; alluvial terrace; growth-strata; piedmont.

Abstract

We document the temporal evolution of deformation in the northern Tianshan piedmont where the deformation is partitioned across several thrusts and folds. We focus on the Dushanzi anticline, where abandoned terraces and growth strata allow us to document the history of folding since the Miocene to be documented. Based on subsurface seismic imaging, structural measurements and a morphological analysis, we show that this anticline is associated with two decollement levels. We use kink band migration in growth strata dated by paleomagnetism to constrain the shortening from the Mio-Pliocene to the Holocene. Our results show that the Dushanzi anticline has been active since at least 8 Ma and that the fold grew at a steady shortening rate of 0.6±0.1 mm/yr mm/yr from 8 to ~1 Ma and then accelerated rapidly to a rate of 4.3±1.0mm/yr over the last 100 ka. These results, together with similar temporal shortening evolutions across other individual structures, suggest that the deformation across the eastern Tianshan piedmonts increased relatively recently. This may reflect either a redistribution of the deformation from the internal structures toward the borders or a general acceleration of the deformation across the entire range.

1/Introduction

The Tianshan is a major mountain range that reaches elevations of over 7000m and dominates the topography of central Asia. The range extends over a distance >1500 km, with both width and average elevation decreasing from west to east (Fig.1). In more detail, the topography is composed of a series of elevated ranges (> 4000 m) separated by very large E-W striking

intermontane basins. The overall range rose between the Oligocene and Miocene in response to the India/Eurasia collision, which reactivated numerous structures originally built during earlier Paleozoic collision and subduction episodes (Chen et al., 1999; Dumitru et al., 2001; Gao et al., 1998). Geodetic measurements indicate that in its western part the Tianshan accommodates up to 20 mm/yr, i.e. 40% of the total present-day convergence between India and Asia (Abdrakhmatov et al., 1996; Wang et al., 2001; Yang et al., 2008; Zubovich et al., 2010). The present shortening rate decreases eastward, mimicking the lateral variations in topography and width of the range (Reigber *et al.*, 2001; Wang *et al.*, 2001; Yang et al., 2008), as a consequence of the regional clockwise rotation of the southern Tarim block (Avouac et al., 1993; Yang et al., 2008; Zubovich et al., 2010). At the longitude of this study, the Tianshan range absorbs ~8 mm/yr of shortening between the Junggar and the Tarim basins, which are two large intracontinental and endorheic basins, trapping the sediments shed from the uplifting reliefs. These foreland basins have been affected by intense thin skin tectonics, with folding, thrusting and thickening occurring along both the northern and southern sides of the range. Pleistocene to Holocene deformation can be documented from the deformation of alluvial fans and river terraces (e.g. Avouac et al., 1993; Molnar et al., 1994). The deep structure and deformation over the late Cenozoic can be documented from seismic profiles and from the exceptional exposure of the stratigraphy (Charreau et al., 2008; Daëron et al., 2007; Lu et al., 2010; Stockmeyer et al., 2017, 2014). The Northern piedmont of the eastern Tianshan is therefore a natural laboratory in which to study the temporal evolution of a fold-and-thrust belt. Despite a growing number of studies, at the geological time scale large uncertainties remain regarding the exact distribution of the deformation between the numerous structures that comprise the piedmont. To better understand how the Tianshan grew, more quantitative constraints are thus still needed.

Here, we build on previous studies to document the structure and temporal evolution of deformation across the western part of the northern piedmont(Figs. 1 and 2). At the longitude of our study area, three main folds have been identified/described: (from south to north) the Tuositai anticline, the Dushanzi anticline and the Wusu blind fold (Avouac et al., 1993; Deng et al., 1996; Fu et al., 2003; Li et al., 2010). To the south, the Paleozoic rocks of the high range overthrust these foreland structures via the Frontal Tianshan Thrust (Stockmeyer et al., 2014). We focus our analyses on the Dushanzi anticline because it represents the main active structure at this particular longitude and has likely undergone most of the deformation accommodated across the entire northern Tianshan piedmont (Avouac et al., 1993; Poisson and Avouac, 2004; Teng et al., 1996). This fold is currently deforming the Junggar foreland basin and presents a 15-km long and 5-to-7 km wide topographic expression of 800 to 1000 meters maximum height (Figs. 1 and 2). From analyses of warped fluvial terraces or deformed strata, the shortening across this structure was previously constrained to between 1 and 3 mm/yr (Avouac et al., 1993; Burchfiel et al., 1999; Molnar et al.,

1994). However, at the time of these pioneer studies, the age of both the studied morphological markers and deformed strata, and the depth geometry of the fold, were barely known. The ages of the Quaternary formations of the Kuitun valley across this fold are now better constrained (Deng et al., 1996; Malatesta et al., 2017; Poisson and Avouac, 2004), the depositional ages of syn-tectonics sediments have been constrained by magnetostratigraphy from 10.5 Ma to 1 Ma (Charreau et al., 2005), and several new seismic lines have been made available (Chen et al., 2012; He et al., 2005) revealing the depth structure of the fold. These new data have enabled both the short term and long term shortening rates absorbed by the Dushanzi anticline to be better estimated, and have provided new insights into the deformation history of the Northern TianShan piedmont. In the following, based on additional dating of the Kuitun fluvial terraces and a kinematic model of the southern limb of the Dushanzi anticline, we estimate first the recent deformation rates from two folded alluvial terrace treads, and second, the long term deformation from analysis and modeling of the growth strata. We then discuss the distribution and evolution of the deformation across the northern Tianshan piedmont as well as the implications for the evolution of the entire range.

2/Morpho-tectonic settings

2.1 Morphology of the Dushanzi area

The morphology of the Dushanzi area (Fig. 2) is characterized by a large alluvial fan that was probably deposited during the Pleistocene (Guerit et al., 2015; Jolivet et al., 2014; Poisson and Avouac, 2004; Poisson, 2002) (Fig. 2A). The fan was later entrenched by the Kuitun river during the Holocene (Poisson and Avouac, 2004 and Fig. 2A), giving way to the development of a second fan to the north. The latter remains active, trapping most of the sediments currently shed from the high range by the Kuitun River. The entrenchment has left behind numerous paired terraces, which can be mapped on both sides of the river (Fig. 2 and 3) (Poisson and Avouac, 2004, Malatesta et al., 2017). In the upstream part of the section, three main large fill-cut terraces, T11, T10 and T9, can be identified 200 to 300 m above the modern river. These terraces all slope gently northwards at an angle slightly higher than the present river bed (Fig. 4). Across the anticline, only terraces T10 and T12 can be traced (Figs. 2B and 3) (Molnar et al., 1994) in addition to several fill-cut terraces below and younger than T8. T10 and T12 present a convex geometry that is inconsistent with a graded channel slope, suggesting that they have been folded (Fig. 4) (Molnar et al., 1994). In more detail, both terraces show clear and rapid breaks in slope consistent with fold scarps (Fig. 4 and A). However, while terrace T10 shows two breaks and a constant slope between them, terrace T12 presents a third break in the middle. As both surfaces were deformed by the same structure at depth, the discrepancy between the two profiles is not therefore of structural origin. Alternatively, it may

suggest that the abandonment of surface T12 was likely more complex and diachronic (Fig. A and Molnar et al., 1994).

Finally, to the north of this this convex geometry zone, on both the left and right banks of the valley, the river abandoned four wide and flat terraces that slope gently northwards (Fig. 2B). Here it can be seen that terrace T10 appears to merge with the Pleistocene fan level.

Several studies have constrained either the depositional or abandonment ages of the numerous alluvial terraces identified across the Kuitun valley (Molnar et al., 1994; Poisson and Avouac, 2004; Malatesta et al., 2017 Fig. 2B). Here, we focus our analyses on T10 and T12 because these are, respectively, the most continuous and highest terraces preserved across the fold and may therefore provide the best and longest records of the deformation.

From cosmogenic analyses of four surface cobbles, Molnar et al. (1994) constrained the abandonment age of T12 south of the Dushanzi anticline to between 14 and 44 ka. They also sampled four surface cobbles on the same surface where tilted in the back limb of the fold, constraining the ages to between 41 and 178ka (Fig. 2). These exposure ages remain loose however, as in addition to the low number of samples and the wide data dispersion, they do not account for inheritance bias (see the supplementary information section for a discussion of this critical issue). Moreover, they were obtained 20 years ago, and thus require new calibration updates. From OSL analyses, Poisson (2002) constrained the deposition of this terrace to 86 ka. However, these analyses were performed on a multi-grain single aliquot. To better account for the variable and incomplete bleaching that is highly probable in such a fluvial setting, we carried out single-grain post-infrared infrared stimulated luminescence (p-IR IRSL) dating of K-feldspar grains (e.g. Thiel et al., 2011). The sample was taken at the base of a 10-m-thick loess layer that tops terrace T12, 40 cm above the contact between the loess and the alluvial pebbles of the terrace. After digging 50 cm deep to avoid any potential colluvium contamination from the surface, the loess was sampled in a metallic pipe and rapidly shielded with black tape. Three additional loess samples were taken at a distance of 30 cm from the OSL tube for radiogenic element measurements. Details of the sample treatment and measurements are given in the online repository data. The final age obtained after correction for fading is 116.1±14.8 ka. As this dating was performed on the loess cover that seals the terrace deposit it should be considered a minimum estimate of the terrace abandonment age. Nevertheless, it is to the first order coherent with the revised cosmogenic exposure ages of the four surface cobbles sampled and analyzed by Molnar et al. (1994) on the tilted surface located on the backlimb of the fold (Fig. 4).

The exposure age of T10 was initially constrained to be between 8 and 22ka using cosmogenic analyses of five surface cobbles (Molnar et al., 1994). On the basis of a cosmogenic depth profile analysis that accounts for the inheritance bias, we find that T10 was likely abandoned

between 6 and 14 ka (see Supplementary information). However, simulated luminescence-based analyses provide a better constraint on the depositional age of this terrace. From OSL analyses, Poisson and Avouac (2004) constrained the timing of its deposition to between 7 and 11 ka. Malatesta et al. (2017) used single grain post Infra-Red Infra-Red Stimulated Luminescence (pIR-IRSL) to analyze a new sample collected near the first OSL sampling site (Fig. 2), and revised the depositional age of T10 to 13.4±1.6 ka.

2.2/ Structure of the Dushanzi Anticline

The detailed structure of the Dushanzi anticline was revealed by the entrenchment of the Kuitun River, a process that left behind continuous outcrops of the folded strata. Bedding attitudes were therefore measured at more than 350 sites along the section and reveal a fairly uniform strike but a change in dip, highlighting the existence of an anticline fold (Figs. 3 and 5). In the northern limb, the south dipping fault reaches the surface and even affects the surface of the young Holocene alluvial fan, as evidenced by a 5-km-long east-west striking fault scarp (Avouac et al., 1993; Deng et al., 1996). Accordingly, the Dushanzi anticline was first described in the literature to be a simple fault bend fold rooted in a single detachment layer that reaches the surface and was recently active (Avouac et al., 1993; Deng et al., 1996; Burchfiel et al., 1999). However, the deep structure revealed by the seismic line is more complicated (see Fig. 5 and the online depository). In the hanging wall of the fault, the deeper reflectors show no significant bed thickness variations and can be assumed parallel a curved fault ramping up from a subhorizontal décollement at depth. This décollement likely lies in the Jurassic, where several/numerous levels of coal and clay exist (e.g. BRGMX, 1985; Hendrix et al., 1992). The bedding of these reflectors shows a two-step change in attitude. This suggests the existence of two hinge zones bounded by four axial surfaces (Fig. 4b). This ramp is probably linked to the major thrust at depth that extends below the range ~15 km to the south (Stockmeyer et al., 2014).

However, this deep décollement can hardly be connected to the fault that breaks through at the surface. Moreover, the short wavelength anticline geometry (<2km) revealed by the surface dip measurements cannot be related to the deep larger scale structure inferred in the seismic line (>5km). It is worth noting that the deep structure of the Dushanzi anticline is not expressed in the actively folded landscape. The emersion of the upper ramp, as evidenced by the fault scarp (Figs. 3, 4 and 5), suggests that the deep fold structure is no longer active. A décollement at a higher structural level has more recently been activated, and likely accommodates the present deformation. By analogy with nearby sections (Li et al., 2011; Stockmeyer et al., 2014), this décollement is probably located in the silt rich and lacustrine Anjihai formation of late Paleocene age (BRGMX, 1985; Charreau et al., 2009). Thus, we hypothesize that the thrust follows this formation and parallels the

strata along the back limb of the fold (Fig. 5). Its geometry therefore follows the reflectors at depth and is likely similar to the lower ramp. It likewise includes two step changes in bedding attitude and is rooted in the southern part of the section.

In conclusion, we interpret the geometry of the Dushanzi fold to be a fault-bend-fold anticline with two levels of décollement. In the footwall of this structure, the bedding attitudes are fairly uniform and relatively flat.

3/ Shortening rates across the Dushanzi anticline

3.1/ Kinematic model

The geometry of any layer deformed across a fold can be modelled using a simple geometric formulation of the displacement by assuming that fold growth is controlled by a curved hinge kink-band migration (Suppe et al., 1997). In such a model, the hinge zone has a finite width and is limited by entry and exit axial surfaces (Charreau et al., 2008). The folding and the rotation of the layers are only acquired inside the hinge zone through the hanging wall (Suppe et al., 1997). The geometry of any layer that crosses the hinge zone can be easily computed from a series of equations (See Appendix of Charreau et al., 2008) that rely on the shortening undergone by the modelled strata, S, the radius of curvature of the hinge zone, Rc, and the opening angle of the curved fold, β (Fig. B in the Online depository information). In such a model, the width of the hinge zone is related to the radius of curvature and the opening angle (Fig. C).

In the Dushanzi anticline, this simple model is complicated by the presence of two imbricated faults. The folding of the layers could have therefore resulted from shortening across one of the two faults or across both faults. It was likely produced in two steps, first by progressive thrusting on the lower ramp and then by later activation of the upper décollement. However, the bedding and rotation of the layers were progressively acquired only within the two hinge zones of the two faults as the layers moved forward. Because the seismic reflectors are strictly parallel at depth, the two fault ramps have very similar geometry with similar radius of curvature and opening angle. The rotation experienced by the lower ramp would be equivalent to that on the upper ramp for the same shortening and vice-versa. Therefore, we limited our modeling to the upper fault assuming it represents the cumulative shortening on both ramps equivalent to a scenario that would include deformation on both ramps.

In our model the dip angles of this ramp were thus set to ~30° and ~8° in the northern and southern parts, respectively. These values mimic the dip of the seismic reflectors at depth and respect the dip measurements at the surface. As the location of the fault at the surface is known, only the depth of the décollement was then adjusted to ~2700m at the southern limit of the seismic line. Finally, the width of the hinge zone was set to ~3500m to respect the rapid elevation changes in

212 the topographic terrace profiles of T10 and T12 (Fig. 4). Indeed, these topogrpahic changes should
213 correspond to fold scarps that reveal the location of the hinge zone at the surface (Fig. A). The radius
214 of curvature derived from this setting is ~7200m. Our modelled upper ramp reproduces the deep
215 reflectors well, respecting their curvature at depth as well as the surface topography (i.e. the
216 terraces).
217
218 *3.2 Long term deformation rates*
219 To constrain the deformation rate over a longer time scale, we first modelled the strata
220 present at depth. However, the quality of the seismic line in the upper part is poor, showing only a
221 few reflectors The modelled strata were therefore compared to the bedding measured at the surface
222 only. These measurements represent the finite result of the shortening on both ramps. To avoid the
223 short wavelength dip variations likely due to measuring biases, we smoothed the data using a 3rd
224 degree polynomial fit. We considered only the southern limb of the Dushanzi anticline where the
225 bedding attitudes decrease progressively. In the northern part, the dip angles result from a more
226 complex deformation process. The shortening of each of the modelled layers was then adjusted to
227 minimize the misfit between the smoothed dip angles at the surfaces and the modelled dip angles
228 (Fig. 6). To derive the history of shortening (Fig. 6), the stratigraphic ages of the modelled horizons
229 were constrained from their horizontal positions along the present river, where the strata have been
230 dated by magnetostratigraphy to be 10.5 to 1.3 My in age (Charreau et al., 2005). Our results suggest
231 continuous and relatively steady fold growth since at least 8Ma, with an overall average shortening
232 rate of ~0.6±0.1 mm/yr. A possible deceleration of the deformation between 2 and 1Ma is however
233 possible.
234
235 *3.3 Pleistocene shortening rates from warped terrace*
236 Based on the same calculations of the displacement and geometry of the upper ramp, we
237 modelled the warped T12 and T10 terrace treads (Fig. 4). In this case, the modelled terraces will
238 depend mainly on the shortening they have undergone and their initial geometry prior to
239 deformation. The latter should mimic the graded long profile of the river system that created the
240 geomorphic markers. Thus, similar to the present river, we assume that the elevation change of the
241 initial terraces might be approximated by a linear or smoothly evolving profile (Fig. 4). This can be
242 defined using the marker geometry in zones that underwent only uplift and translation but no
243 rotation, unlike in the hinge area (*e.g.* Molnar *et al.*, 1994). The initial slope of terrace T10 before its
244 deformation was thus defined by a linear profile from the DGPS data in the zone uplifted above the
245 steepest part of the ramp, located north of the hinge zone (abscissa ~4000m to ~6500m). In contrast,

246 the initial slope of terrace T12 was defined in the southern part of the profile, south of the hinge
247 zone (abscissa ~-2000m to ~0m).
248 Terrace T10 shows only two breaks in slope that are consistent with the structure at depth.
249 This surface must have been abandoned and then deformed without sediment aggradation in the
250 back limb (Fig. 4 and A). The original position of the terrace was therefore restored by a simple
251 translation that depends on the shortening S. The original profile was then deformed across the
252 entire ramp according to the same shortening and using our kink band migration model to fit it to the
253 elevation data of the terrace. Based on a least square adjustment, we found that a shortening of
254 ~57m yields an overall modelled profile shape that is relatively consistent with the elevation change
255 of the terrace (Fig. 4).
256 The modelling of terrace T12 was complicated by the presence of the third break in slope located
257 within the hinge zone. This likely reflects/represents a diachronism of the surface due to a phase of
258 sediment aggradation in the back limb of the fold, followed by incision and abandonment (Molnar et
259 al., 1994, Fig. A). Therefore, following the Molnar et al. (1994) scenario, and based on our new pIRSL
260 dating, we assumed that the surface was first abandoned and uplifted at ~116 ka north of the hinge
261 zone. Within and south of the hinge zone, this surface remained partially buried at first due to
262 sediment aggradation as the Pleistocene fan grew. The entire surface was then abandoned because
263 aggradation had stopped and incision started, or at least because the sedimentation was insufficient
264 to compensate for uplift. The total shortening S, the sediment aggradation rate a_r and the time when
265 aggradation stopped t_{ab} were then adjusted to fit to the elevation data by minimizing the Mean
266 Square Deviation (MSD) (Fig. 4). We obtained values of 518m, 26ka and 0.7mm/yr for S, t_b and a_r,
267 respectively. However, a_r and t_b remain first order estimates and should be treated with caution as
268 we assumed in our scenario that the aggradation was continuous and steady while it is possible that
269 it varied over time. However, our abandonment age remains broadly consistent with the revised
270 exposure age of the surface cobble sampled and analysed by Molnar et al. (1994) (Fig. 4). The total
271 shortening value is more robust because it relies only on the steepest part of the profile. This area
272 represents the original abandoned surface and has recorded the full shortening and rotation within
273 the hinge zone.
274 For both terraces, we attached a large conservative uncertainty of 20% to our shortening
275 values to account for possible errors in the seismic line location and its projection with respect to the
276 terrace profile. Based on the terrace ages of 116.1±14.8 ka (this study) and 13.4±1.6 ka (Malatesta et
277 al., 2017), the shortening rates for T12 and T10 are 4.5±1.0mm/yr and 4.2±1.0 mm/yr, respectively.
278
279 **4/Discussion**
280 *4.1 Depth structures and folding mechanism*

Our shortening estimates, and hence the deformation rates, rely on a fold model that results from our interpretation of the fold structure at depth. Both the interpretation and the model must therefore be questioned to ensure the robustness of our results. Hitherto interpreted as a simple unique fold bend fault (Avouac et al., 1993, Burchfiel, et al., 1999), the deep image of the Dushanzi anticline combined with the fault scarp location and the landscape relief revealed a more complex structure that we interpret as a double thrust of similar dip angle. This interpretation, though relatively unusual, is quite consistent with the cross-sections of He et al., (2005) and Lu et al., (2007) both of which were derived from parallel nearby seismic profiles. Moreover, two levels of décollement are similarly described in a number other anticlines in this piedmont as well as in the southern piedmont (e.g. He et al., 2005; Charreau et al., 2008; Guan et al., 2009; Li et al., 2011, Stockmeyer et al., 2014). In accordance with the terrace geometry, we also assumed that the shortening first started on the lower Jurassic detachment and then shifted to the upper late Paleocene décollement (Fig. 4b-d). This is also consistent with the structural mechanism proposed by He et al. (2005) for the same anticline.

However, while the general kinematics of our fold model are consistent with the literature and other structures in the region, the displacement formulation used is simplistic and the related assumptions might be therefore be questioned We note for example that the few reflectors observed at shallow depth are dipper than the modelled strata (Fig. 6a). However, this discrepancy is likely due to the velocity-time data used to migrate the profile. Indeed, in this part of the section the srata are mainly constituted by the coarse conglomeratic Xiyu formation where the seismic velocity is likely higher than the profile average velocity used for the migration. Consequently, the reflectors were flattened during the migration. It is however difficult to account for such lateral variation of the velocity. More importantly, a significant portion of the strata dip angle may have been acquired by a limb rotation and not only through hinge translation. Likewise, the differential compaction of growth strata might tend to increase the dip angle of the strata and hence have had a similar effect. In a study across the nearby Huerguosi anticline, Charreau et al. (2008) showed that the impact of compaction is probably insignificant compared to the other, larger, uncertainties, especially those associated with the dip angle measurements. All of the terraces show a gentle northward slope slightly higher than that of the present river bed, while a significant limb rotation should have tilted these surfaces southward. This suggests that the impact of limb rotation was limited during the more recent evolution of the fold (i.e. <100ka). However, the question remains open at the longer timescale, especially at the time when the deformation started and when the fold nucleated, likely as a detachment fold. Overwhelming a possible rotation would lead to the overestimation of the long term shortening rate, which is already relatively low.

316 *4.2 Deformation rate variations in the Tianshan piedmonts*

317 Our results suggest that the Dushanzi anticline grew continuously at the same rate during the
318 Mio-Pliocene and then slowed down between 2 and 1Ma. If true, this deceleration would imply that
319 during this period of time, part of the shortening accommodated across the Dushanzi anticline was
320 absorbed across other structures, either more frontal, such as the Wusu anticline, or located further
321 back, such as the Tutsoi anticline (Figs. 1 and 5). However, our results for the 2-1Ma period are weak
322 because, in this part of the section, the lithology is composed of the thick coarse conglomerate Xiyu
323 formation in which precise estimation of the bedding attitude is difficult. Our dip measurements, and
324 thus also our derived shortening rates, are therefore associated with a large uncertainty in this
325 particular zone. The strong acceleration observed during the Pleistocene is more robust. The
326 deformation history of the Dushanzi anticline can be compared to the shortening recorded across
327 other folds on the piedmont. In the Anjihai anticline, located 50km along strike to the west (Fig. 1),
328 Daëron et al., (2007) estimated from fold modeling that the deformation across this detachment fold
329 started at 7.4Ma at a shortening rate of 0.4 mm/yr and continued at this rate until 0.9 Ma, when it
330 accelerated to 1.12 mm/yr. From analysis of a folded terrace, Fu et al. (2017) found that the same
331 anticline shortened at a rate of 0.4-0.7mm/yr between 53ka and 9ka and at a rate of 1.1-1.4 mm/yr
332 since 9ka. The deformation history is therefore relatively similar across both folds but the
333 deformation remains weaker in the Anjihai anticline. This is likely linked to the growth of the
334 Huerguosi anticline located to the south of the Anjihai (Fig. 1). This fault-bend fold was also active
335 during this period of time, accommodating 0.84 mm/yr and 1.14 mm/yr of shortening, from 10 to 4
336 Ma and from 4 Ma to present, respectively (Charreau et al., 2008). Since the Anjihai and Huerguosi
337 anticlines are parallel and are located at the same longitude, their deformations can be summed. This
338 yields a total shortening of ~0.8 mm/yr, which progressively accelerated to ~2.3 mm/yr. These values
339 are lower than our own estimates across the Dushanzi anticline. The difference between the two
340 sections may reflect the existence of active structures south of the Huerguosi anticline (Fig. 1). In the
341 Tugulu anticline, located ~100km east of our study area (Fig. 1), based on an analysis of folded
342 terrace, Stockmeyer et al. (2017) reported deformation rates that decrease from ~4 to ~1mm/yr at
343 the Holocene transition. However, the Neogene rates remain unknown across this fold. Moreover,
344 similar acceleration has also been observed across several individual folds located in the southern
345 Tianshan piedmont at the same longitude (Hubert-Ferrari et al., 2007; Saint-Carlier et al., 2016). The
346 total deformation across this piedmont and the evolution of this deformation though time have not
347 yet been accurately constrained. Taken together, the existing data suggest a 3- to 4-fold acceleration
348 in the deformation within the Tianshan piedmonts sometime between the Neogene and the
349 Pleistocene (Fu et al., 2017). More studies are needed to unambiguously confirm this acceleration,
350 and our conclusion must be therefore be handled with caution, however if it is correct, the

acceleration may have several origins. It may reflect a redistribution of the deformation from the inner toward the more external structures of the orogen. If it is assumed that the present shortening rate derived from GPS (Yang et al., 2008) of ~8.5mm/yr across the range remained constant during the Neogene, then <10% of this total crustal deformation would have been initially accommodated within the northern Tianshan piedmont. Since the Holocene, the value would have increased to up to ~50%. At this longitude, a significant part (>15 %) of the total present crustal shortening across the range is accommodated in the internal part the range (Charreau et al., 2017). Accordingly, the Eastern Central Tianshan is thickening at a rate that is significantly faster/higher than the average denudation rates, suggesting that the Tianshan range has not yet reached a steady topography and remains in a transient state of growth. Such acceleration and redistribution of the deformation toward the piedmont may suggest evolution of the orogen toward a more steady topography in which deformation is progressively being focused at the borders, as observed in other large and more mature orogenic belts such as in the Himalayas (Lavé and Avouac, 2001). Such a redistribution of the deformation may be also forced by sedimentation-tectonic interactions within the piedmont. Indeed, syn-tectonic sedimentation across an active fold may overload the fault, increase the shear stress and influence the geometry and kinematics of the folding (Barrier et al., 2013; Fillon et al., 2013; Mugnier et al., 1997). As soon as the uplift rate due to folding outpaces the sedimentation rate, the fold emerges at the surface and the shear stress decreases thereby strengthening the deformation.

Conclusions

In the Kuitun section, surface geology and morphology as well as seismic imaging at depth reveal a complex fault-bend-fold system composed of two fault related folds, where only the upper structure has actively deformed the landscape. Several alluvial terraces were deposited, abandoned and subsequently deformed across this fold. Though somewhat loose and associated with large uncertainties, our new CRN direct dating of the main terrace, T10, suggests this surface was abandoned between 6 and 15 kyr, in agreement with the initial luminescence age of 13.6 ka of Malatesta et al. (2017). We also provide new pIRSL age for the upper terrace, T12, which constrain its abandonment age to 116.1±14.8 kyr.

Based on a simple geometric formulation of the displacement, we modelled both the pre-growth strata and the growth strata, integrating the geometry of these two deformed and dated alluvial terraces. This work highlights the presence of growth strata on the Dushanzi fold since at least 9 Ma. We also propose that the Dushanzi anticline has shortened at a maximum rate of ~0.7 mm/yr since at least ~7 Ma and that this rate recently (<1Ma ?) accelerated to ~4 mm/yr. While this method can be applied to complex and mature structures such as the Dushanzi anticline, it neglects

possible rotation mechanism and may therefore overestimate the deformation rates. Investigation of the temporal evolution of folding and thrusting of other structures in the northern and southern Tianshan piedmont will help determine if the temporal variations in deformation are due to local interaction between neighbouring structures or to a regional evolution that could be related to the effects of climate-driven erosion and sedimentation, purely tectonic processes, or geodynamics at the regional scale.

Acknowledgements

This study was financed by the French INSU/CNRS SYSTER program. We are grateful to Robert Joussemet (STEVAL mineral processing pilot plant, LEM, Nancy) for his help in separating quartz and to the ASTER team for the cosmogenic nuclide concentration measurements (M. Arnold, G. Aumaître, K. Keddadouche, L. Léanni and F. Chauvet). The ASTER national AMS facility (CEREGE, Aix en Provence) is supported by the INSU/CNRS, the French Ministry of Research and Higher Education, IRD and CEA. This is CRPG contribution n° XXXX.

Bibliography

Abdrakhmatov, K.Y., Aldazhanov, S.A., Hager, B.H., Hamburger, M.W., Herring, T.A., Kalabaev, K.B., Makarov, V.I., Molnar, P., Panasyuk, S. V, Prilepin, M.T., Reilinger, R.E., Sadybakasov, I.S., Souter, B.J., Trapeznikov, Y.A., Tsurkov, V.Y., Zubovich, A. V, 1996. Relatively recent construction of the Tien Shan inferred from GPS measurements crustal deformation rates. Nature 384, 450–453.

Avouac, J.P., Tapponnier, P., Bai, M., You, H., Wang, G., 1993. Active Thrusting and Folding Along the Northern Tien-Shan and Late Cenozoic Rotation of the Tarim Relative to Dzungaria and Kazakhstan. J. Geophys. Res. Earth 98, 6755–6804. doi:Doi 10.1029/92jb01963

Barrier, L., Nalpas, T., Gapais, D., Proust, J., 2013. Impact of synkinematic sedimentation on the geometry and dynamics of compressive growth structures : Insights from analogue modelling. Tectonophysics 608, 737–752. doi:10.1016/j.tecto.2013.08.005

BRGMX, 1985. Geological map of the Xinjiang Uygur Autonomous Region, China. China Geol. Print. House.

Burchfiel, B.C., Brown, E.T., Deng, Q., Li, J., Feng, X., Molnar, P., Shi, J., Wu, Z., You, H., 1999. Crustal Shortening on the Margins of the Tian Shan, Xinjiang, China. Int. Geol. Rev. 41, 663–700.

Charreau, J., Avouac, J.-P., Chen, Y., Dominguez, S., Gilder, S., 2008. Miocene to present kinematics of fault-bend folding across the Huerguosi anticline, northern Tianshan (China), derived from structural, seismic, and magnetostratigraphic data. Geology 36, 871–874. doi:10.1130/G25073A.1

421 Charreau, J., Chen, Y., Gilder, S., Dominguez, S., Avouac, J.-P., Sen, S., Sun, D., Li, Y., Wang, W.M.,
422 2005. Magnetostratigraphy and rock magnetism of the Neogene Kuitun He section (northwest
423 China): Implications for Late Cenozoic uplift of the Tianshan mountains. Earth Planet. Sci. Lett.
424 230, 177–192. doi:10.1016/j.epsl.2004.11.002
425 Charreau, J., Gumiaux, C., Avouac, J.-P., Augier, R., Chen, Y., Barrier, L., Gilder, S., Dominguez, S.,
426 Charles, N., Wang, Q., 2009. The Neogene Xiyu Formation, a diachronous prograding gravel
427 wedge at front of the Tianshan: Climatic and tectonic implications. Earth Planet. Sci. Lett. 287,
428 298–310. doi:10.1016/j.epsl.2009.07.035
429 Charreau, J., Saint-Carlier, D., Dominguez, S., Lavé, J., Blard, P.-H., Avouac, J.-P., Jolivet, M., Chen, Y.,
430 ShengLi, W., Borwn, N.D., Malatesta, L.C., Rhodes, E., Team, A., 2017. Denudation outpaced by
431 crustal thickening in the eastern Tianshan. Earth Planet. Sci. Lett. in press.
432 Chen, C., Lu, H., Jia, D., Cai, D., Wu, S., 1999. Closing history of the southern Tianshan oceanic basin,
433 western China: an oblique collisional orogeny. Tectonophysics 302, 23–40.
434 Chen, W., Hao, J.J., Li, S.Q., Peng, W.L., Xian, D., Chen, L.H., Li, Z.G., 2012. The geometric and
435 kinematic numerical simulation of the Dushanzi anticline, southern Junggar Basin. Chinese J.
436 Geol. 47, 37–50.
437 Daëron, M., Avouac, J.-P., Charreau, J., 2007. Modeling the shortening history of a fault tip fold using
438 structural and geomorphic records of deformation. J. Geophys. Res. 112, B03S13.
439 doi:10.1029/2006JB004460
440 Deng, Q., Zhang, P., Xu, X., Yang, X., Peng, S., Feng, X., 1996. Paleosismology of the northern
441 piedmont of Tianshan Moutains, northwesr China. J. Geophys. Res. 101, 5895–5920.
442 Dumitru, T.A., Zhou, D., Chang, E.Z., Graham, S.A., Hendrix, M.S., Sobel, E.R., Caroll, A.R., 2001. Uplift,
443 exhumation, and deformation in the Chinese Tian Shan, in: Hendrix, M.S., Davis, G.A. (Eds.),
444 Paleozoic and Mesozoic Tectonic Evolution of Central Asia : From Continental Assembly to
445 Intracontinental Deformation. Geological Society of America Memoir 194, Boulder : colorado,
446 pp. 71–99.
447 Fillon, C., Huismans, R.S., van der Beek, P., 2013. Syntectonic sedimentation effects on the growth of
448 fold-and-thrust belts. Geology 41, 83–86. doi:10.1130/G33531.1
449 Fu, B., Lin, A., Kano, K., Maruyama, T., Guo, J., 2003. Quaternary folding of the eastern Tian Shan,
450 northwest China. Tectonophysics 369, 79–101.
451 Fu, X., Li, S., Li, B., Fu, B., 2017. A fluvial terrace record of late Quaternary folding rate of the Anjihai
452 anticline in the northern piedmont of Tian Shan , China. Geomorphology 278, 91–104.
453 doi:10.1016/j.geomorph.2016.10.034
454 Gao, J., Li, M., Xiao, X., Tang, Y., He, G., 1998. Paleozoic tectonic evolution of the Tianshan Orogen,
455 northwestern China. Tectonophysics 287, 213–231.

Guerit, L., Barrier, L., Jolivet, M., Fu, B., Métivier, F., 2015. Denudation intensity and control in the Chinese Tian Shan: new constraints from mass balance on catchment-alluvial fan systems. Earth Surf. Process. Landforms n/a–n/a. doi:10.1002/esp.3890

He, D., Suppe, J., Geng, Y., Shuwei, G., Shaoying, H., Xin, S., Xiaobo, W., Chaojun, Z., 2005. Guide book for field trip in south and north Tianshan foreland basin, Xinjiang Uygur Autonomous Region, China, in: International Conference on Theory and Application of Fault-Related Folding in Foreland Basins. Beijing, p. 77.

Hendrix, M.S., Graham, A.S., Carroll, A.R., Sobel, E.R., McKnight, C.L., Schulein, B.J., Wang, Z., 1992. Sedimentary record and climatic implications of deformation in the Tian Shan : Evidence from Mesozoic strata of the north Tarim, south Junggar, and Turpan Basins, northwest China. Geol. Soc. Am. Bull. 104, 53–79.

Hubert-Ferrari, A., Suppe, J., Gonzalez-Mieres, R., Wang, X., 2007. Mechanism of active folding of the landscape (southern Tianshan, China). J. Geophys. Res. 112, doi: 10.129/2006JB004362.

Jolivet, M., Barrier, L., Dominguez, S., Guerit, L., Heilbronn, G., Fu, B., 2014. Unbalanced sediment budgets in the catchment-alluvial fan system of the Kuitun River (northern Tian Shan, China): Implications for mass-balance estimates, denudation and sedimentation rates in orogenic systems. Geomorphology 214, 168–182. doi:10.1016/j.geomorph.2014.01.024

Lavé, J., Avouac, J.P., 2001. Fluvial incision and tectonic uplift across the Himalayas of central Nepal. J. Geophys. Res. 106, 26561. doi:10.1029/2001JB000359

Li, C., Guo, Z., Dupont-nivet, G., 2011. Cenozoic tectonic deformation across the northern foreland of the Chinese Tian Shan. J. Asian Earth Sci. 42, 1066–1073. doi:10.1016/j.jseaes.2010.08.009

Li, C., Guo, Z., Dupont-nivet, G., 2010. Late Cenozoic tectonic deformation across the northern foreland of the Chinese Tian Shan. J. ASIAN EARTH Sci. doi:10.1016/j.jseaes.2010.08.009

Lu, H., Burbank, D.W., Li, Y., 2010. Alluvial sequence in the north piedmont of the Chinese Tian Shan over the past 550 kyr and its relationship to climate change. Palaeogeogr. Palaeoclimatol. Palaeoecol. 285, 343–353. doi:10.1016/j.palaeo.2009.11.031

Malatesta, L.C., Avouac, Jean-Philippe Brown, N.D., Breitenbach, S.F.M., Pan, J., Chevalier, M.-L., Rhodes, E., Saint-Carlier, Dimitri Zhang, W., Charreau, J., Lavé, J., Blard, P.-H., 2017. Lag and mixing during sediment transfer across the Tian Shan piedmont caused by climate-driven aggradation-incision cycles. Bull. Geol. Soc. Am. In press.

Molnar, P., Brown, E.T., Burchfiel, B.C., Deng, Q., Feng, X., Li, J., Raisbeck, G.M., Shi, J., Wu, Z., Yiou, F., You, H., 1994. Quaternary Climate Change and the Formation of River Terraces across Growing Anticlines on the North Flank of the Tianshan, China. J. Geol. 102, 583–602.

Mugnier, J.L., Baby, P., Français, I., Préau, D.B., Géodynamique, L. De, Gignoux, M., Bale, P., Français, I., Préau, D.B., 1997. Thrust geometry controlled by erosion and sedimentation : A view from

analogue models 427–430.

Poisson, B., 2002. Impact du climat et de la tectonique sur l'évolution géomorphologique d'un piémont : exemple du piémont Nord du Tian Shan depuis la fin du Pléistocène. University of Paris XI, Paris.

Poisson, B., Avouac, J.P., 2004. Holocene hydrological changes inferred from alluvial stream entrenchment in North Tian Shan (Northwestern China). J. Geol. 112, 231–249.

Saint-Carlier, D., Charreau, J., Lavé, J., Blard, P.H., Dominguez, S., Avouac, J.-P., Wang, S., Arnold, M., Aumaître, G., Keddadouche, K., Léanni, L., Chauvet, F., Bourlés, D.L., 2016. Major temporal variations in shortening rate absorbed along a large active fold of the southeastern Tianshan piedmont (China). Earth Planet. Sci. Lett. 434, 333–348. doi:10.1016/j.epsl.2015.11.041

Stockmeyer, J.M., Shaw, J.H., Brown, N.D., Rhodes, E.J., Richardson, P.W., Wang, M., Lavin, L.C., Guan, S., Sciences, S., Angeles, C.L., Young, C., East, D., 2017. Active thrust sheet deformation over multiple rupture cycles : A quantitative basis for relating terrace folds to fault slip rates. Geol. Soc. Am. Bull. 1–20. doi:10.1130/B31590.1

Stockmeyer, J.M., Shaw, J.H., Guan, S., 2014. Seismic Hazards of Multisegment Thrust-Fault Ruptures: Insights from the 1906 Mw 7.4-8.2 Manas, China, Earthquake. Seismol. Res. Lett. 85, 801–808. doi:10.1785/0220140026

Suppe, J., Sabat, F., Munoz, J.A., Poblet, J., Roca, E., Verges, J., 1997. Bed-by-bed fold growth by kink-band migration; Sant Llorenc de Morunys, eastern Pyrenees. J. Struct. Geol. 19, 443–461.

Teng, Z.H., Yue, L.P., Pu, R.H., Deng, X.Q., Bian, X.W., 1996. The magnetostratigraphic age of the Xiyu Formation. Geol. Rev. 42, 481–489.

Thiel, C., Buylaert, J., Murray, A., Terhorst, B., Hofer, I., Tsukamoto, S., Frechen, M., 2011. Luminescence dating of the Stratzing loess pro fi le (Austria) e Testing the potential of an elevated temperature post-IR IRSL protocol. Quat. Int. 234, 23–31. doi:10.1016/j.quaint.2010.05.018

Wang, Q., Zhang, P.-Z., Freymueller, J.T., Bilham, R., Larson, K.M., Lai, X., You, X.Z., Niu, Z.J., Wu, J.C., Li, Y.X., Liu, J.N., Yang, Z.Q., Chen, Q.Z., 2001. Present-day crustal deformation in China constrained by global positioning system measurements. Science (80-.). 294, 574–577.

Yang, S., Jie, L.I., Qi, W., 2008. The deformation pattern and fault rate in the Tianshan Mountains inferred from GPS observations. Sci. China Ser. D-Earth Sci. 51, 1064–1080. doi:10.1007/s11430-008-0090-8

Zubovich, A. V, Wang, X., Scherba, Y.G., Schelochkov, G.G., Reilinger, R., Reigber, C., Mosienko, O.I., Molnar, P., Michajljow, W., Makarov, V.I., Li, J., Kuzikov, S.I., Herring, T.A., Hamburger, M.W., Hager, B.H., Dang, Y., Bragin, V.D., Beisenbaev, R.T., 2010. GPS velocity field for the Tien Shan and surrounding regions 29, 1–23. doi:10.1029/2010TC002772

Table and figure captions

Figure 1: A: Shaded SRTM topography of Central Asia with GPS horizontal velocity (Yang et al., 2008). B: Satellite map of the northern Tianshan foreland showing locations of earthquakes recorded since 1930 (USGS ANSS catalog). Note in particular the recent 5.2 magnitude earthquake that shook this area on 22 February 2015, highlighting the active deformation in the region. The dashed scare indicates the location of our studied area.

Figure 2: A: Geomorphologic and tectonic map of the Dushanzi area, showing the two imbricate fans and the location of the Dushanzi anticline. B: Spot DEM shaded topography showing the locations of the main alluvial terraces identified (T1 to T6). Their identification and mapping (Fig. 2B) were based on Malatesta et al. (2017), who interpretated the terrace morphology from detailed Lidar measurments. The different age data and their associated methods are reported in the white boxes. The dashed line indicates the projection line used to plot the topographic profile in Figure 3. The zero distance corresponds to the southern limit of the seismic profile.

Figure 3: Panorama of the Dushanzi Anticline and its morpho-structural interpretation (bottom)

Figure 4: Topographic profiles of terraces T10 and T12. The elevation across T10 was measured with infra-centimetric accuracy using a differential GPS (black circles). The heights of T12 were measured using a total station theodolithe by Molnar et al. (1994). Both profiles were corrected for the slope of the original abandoned surface (dashed red lines) in order to quantify the uplift they have recorded. The red lines show our best-fitting model and associated shortening estimates. For T10 we also show in light blue and orange two other modelledsurfaces modelled using different values of shortening. For T12 the dashed blue line indicates the geometry of the surface without sediment aggradation. The surface cobble ages were calculated from the data of Molnar et al. (1994) revised using new calibration updates. The inset diagrams show the parameters tested (S, a_r and t_{ab}) against the residual square of the mean.

Figure 5: Simplified cross section of the Northern Tianshan piedmont at the longitude of the Dushanzi anticline with a line drawing of the seismic profile provided by Chen et al. (2012). The structure of the Dushanzi anticline was constrained from seismic subsurface imaging and surface structural measurements. Measured dip angles along the Kuitun River are shown as green segments while the main seismic reflectors are shown in black. The orange line indicates the axial surface used in our fold model.

Figure 6: A: Pre-growth and growth strata predicted by our model using the surface bedding dip adjustment method and comparison with the seismic line drawing (only half of the lines were

drawn; see figure D in the online appendix for a complete view). B: Measured (green circle), smoothed (red line) and modelled (blue circle) dip angles against the horizontal distance along the section. C: temporal evolution of the shortening rates across the Dushanzi anticline for each of the modelled layers. Assuming 5° for the 1σ uncertainty in each individual dip angle measurement, we used the Chi-square criterion to estimate the resulting uncertainty in shortening at the 67% (1σ) confidence level. This uncertainty accounts for measurement errors and for the natural roughness of bedding surfaces. Each age is assigned to a confidence interval corresponding to the chron defined by the magnetostratigraphic data points that bracket the stratigraphic location of the point of interest. However, for each point we assumed a symmetrical uncertainty using the maximum limit. Following the approach developed by York et al. (2004), the average shortening rate and its uncertainty was constrained using a general least-squares procedure that allows the uncertainties in the shortening estimates as well as in the ages to be taken into account. The inset diagram shows the shortening versus time as derived from the modeling of the two warped terraces (see fig. 4).

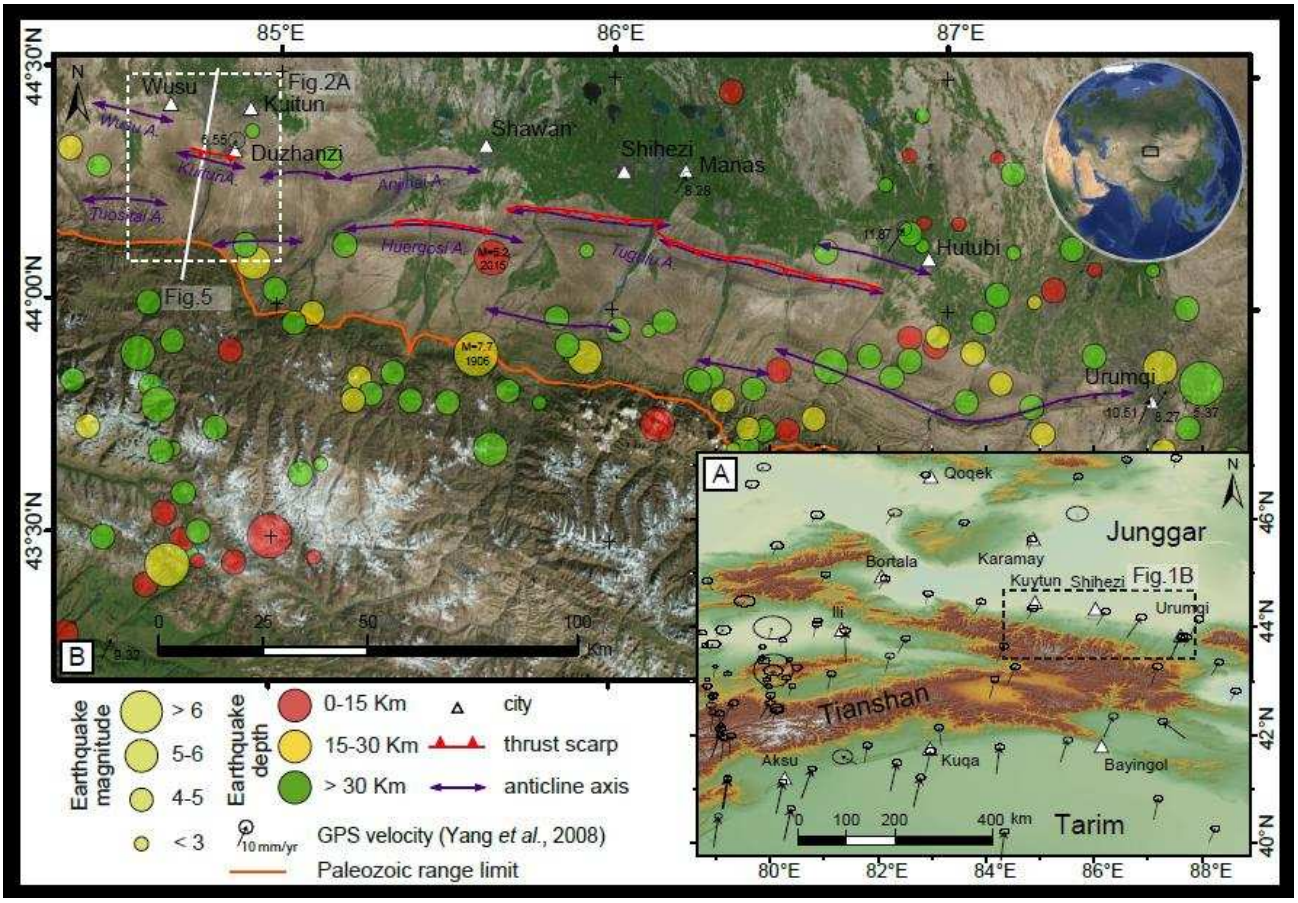

Fig. 1

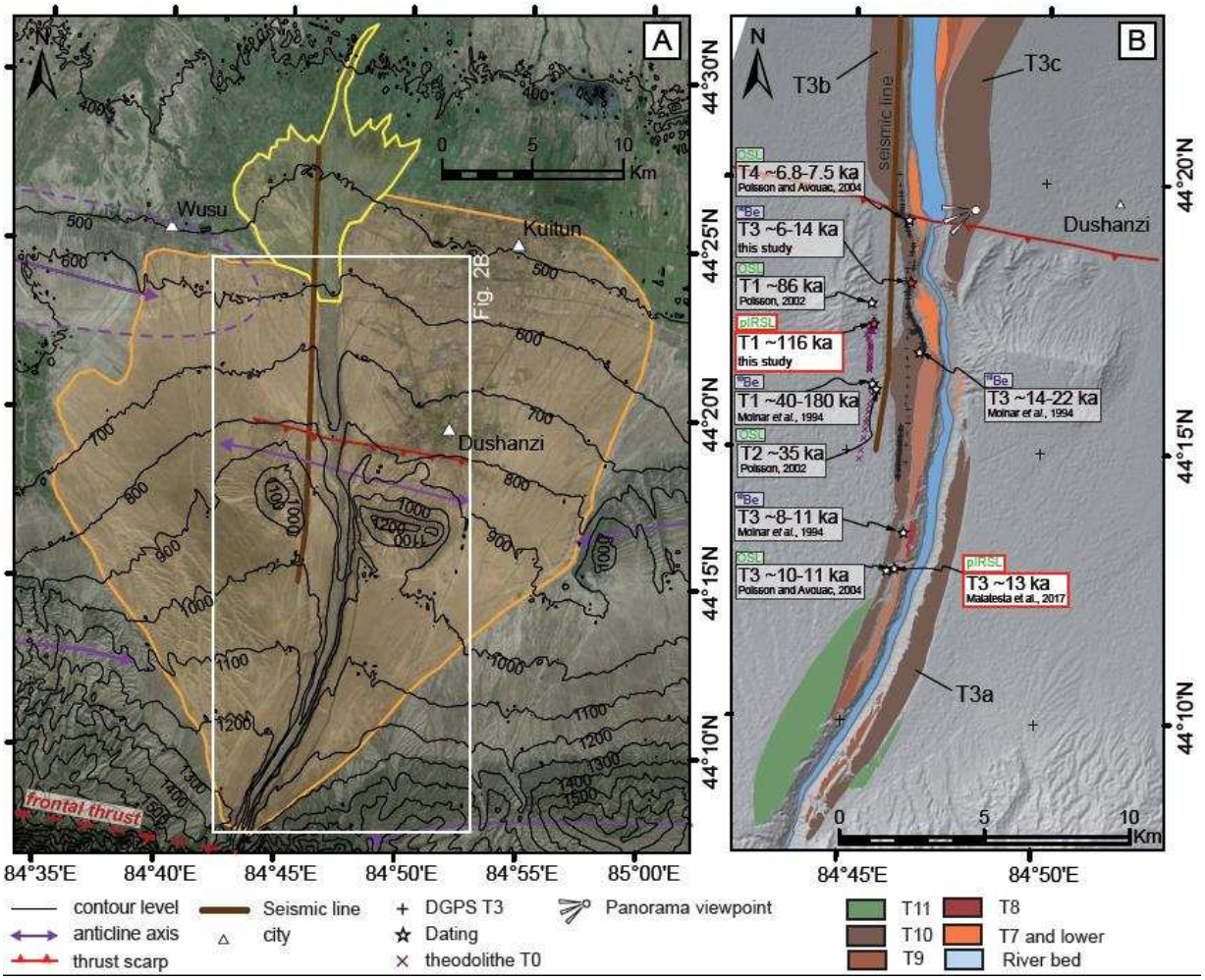

578 Fig. 2

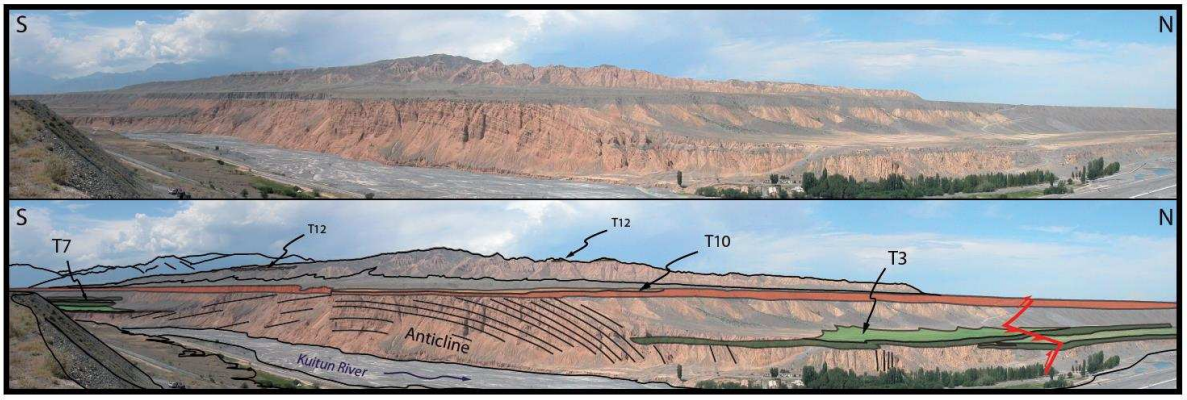

Fig. 3

579

580

581

582

583

584

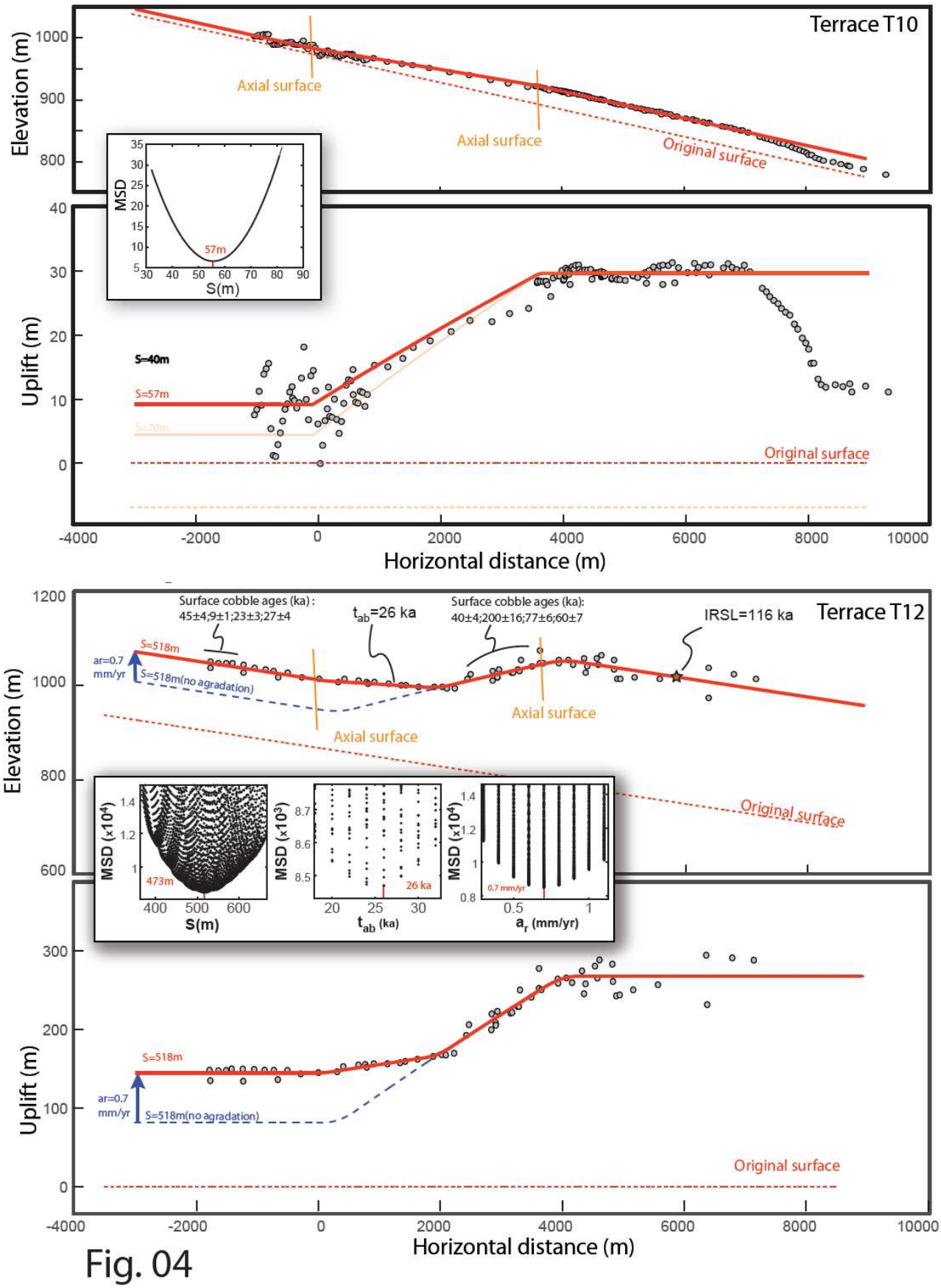

Fig. 04

588

589

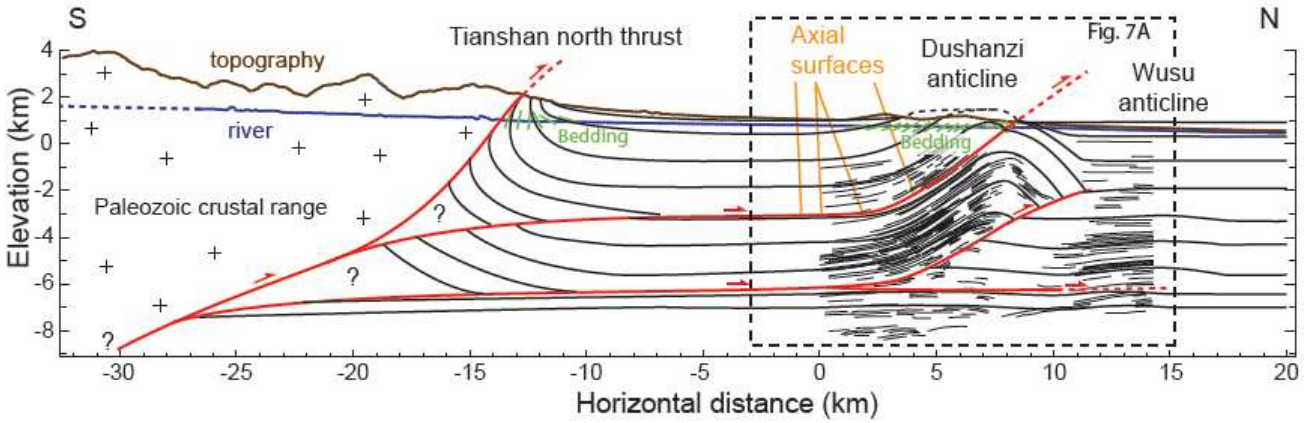
S
N
Tianshan north thrust
topography
river
Paleozoic crustal range
Axial surfaces
Dushanzi anticline
Fig. 7A
Wusu anticline
Bedding
Bedding
Elevation (km)
Horizontal distance (km)

Fig. 05

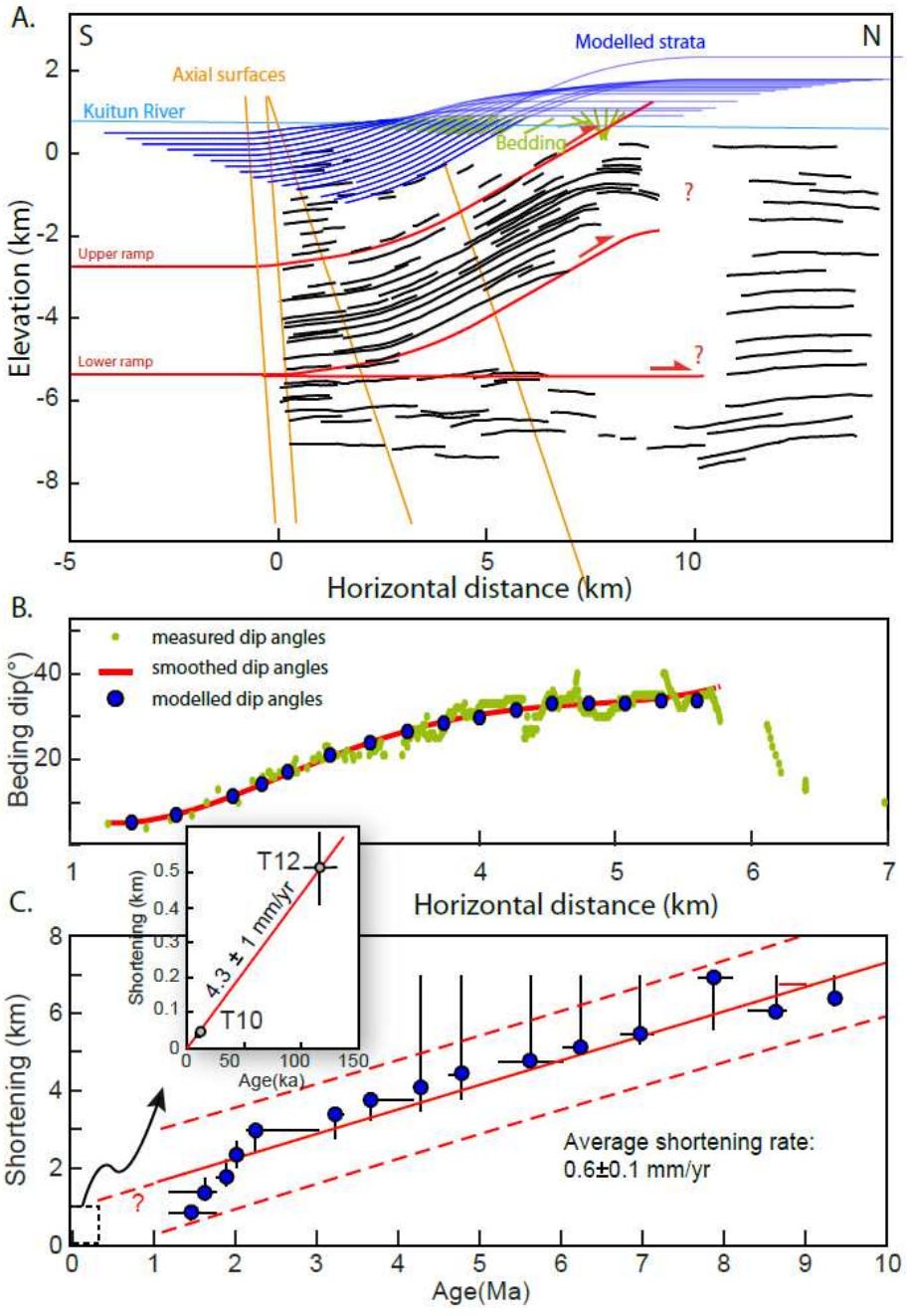
A.
S
N
Modelled strata
Axial surfaces
Kuitun River
Bedding
Upper ramp
Lower ramp
Elevation (km)
Horizontal distance (km)
B.
measured dip angles
smoothed dip angles
modelled dip angles
Beding dip(°)
Horizontal distance (km)
C.
T12
T10
4.3 ± 1 mm/yr
Shortening (km)
Age(ka)
Average shortening rate:
0.6±0.1 mm/yr
Shortening (km)
Age(Ma)

Fig. 6